Electrical detection of coherent ^{31}P spin quantum states

ANDRE R. STEGNER[1]*, CHRISTOPH BOEHME[2,3]*, HANS HUEBL[1], MARTIN STUTZMANN[1], KLAUS LIPS[3] AND MARTIN S. BRANDT[1]

[1]Walter Schottky Institut, Technische Universität München, Am Coulombwall 3, 85748 Garching, Germany
[2]University of Utah, Physics Department, 115S 1400E, Salt Lake City, Utah 84112, USA
[3]Abt. Silizium-Photovoltaik, Hahn-Meitner-Institut Berlin, Kekuléstr. 5, 12489 Berlin, Germany
*e-mail: stegner@wsi.tum.de; boehme@physics.utah.edu

Published online: 19 November 2006; doi:10.1038/nphys465

In recent years, a variety of solid-state qubits has been realized, including quantum dots[1,2], superconducting tunnel junctions[3,4] and point defects[5,6]. Owing to its potential compatibility with existing microelectronics, the proposal by Kane[7,8]—on the basis of phosphorus donors in silicon—has been pursued intensively[9–11]. A key issue of this concept is the readout of the ^{31}P quantum state. Electrical measurements of magnetic resonance have been carried out on single spins[12,13], but the statistical nature of these experiments based on random-telegraph-noise measurements has impeded the readout of single spin states. Here, we demonstrate the measurement of the spin state of ^{31}P donor electrons in silicon and the observation of Rabi flops by purely electric means, that is by coherent manipulation of spin-dependent charge-carrier recombination between the ^{31}P donor and paramagnetic localized states at the Si/SiO_2 interface. The electron spin information is shown to be coupled through the hyperfine interaction to the ^{31}P nucleus, suggesting that recombination-based readout of nuclear spins is feasible.

As the detection of single charges has become technically straightforward, it is widely believed[7,8,10–12] that the realization of spin-to-charge transfer is the key prerequisite for a successful implementation of single spin phosphorus (^{31}P) readout devices, capable of determining the actual spin state (spin up $|\uparrow\rangle$ or spin down $|\downarrow\rangle$). Different approaches to the electrical spin readout of ^{31}P donor electron spins have been proposed on the basis of spin-dependent transitions between neighbouring ^{31}P atoms[7,8,10,11]. As the states involved are energetically degenerate, these spin-to-charge transfer schemes are rather difficult to realize. Alternatively, spin-dependent transitions involving dissimilar paramagnetic states might be easier to detect as proposed by Boehme and Lips[14]. Spin-dependent charge-carrier transport and recombination have been known at least since 1966 (ref. 15), when Schmidt and Solomon observed spin-dependent recombination involving ^{31}P donors in silicon. However, it was not demonstrated until 2003 (ref. 16) that the much more sensitive electrical detection of spins via resonant changes of recombination processes is also able to reflect coherent spin motion, which is necessary for a readout of the spin quantum state as opposed to a mere detection of the presence of spins.

Figure 1a shows the readout scheme on the basis of spin-dependent recombination demonstrated in this paper. To probe ^{31}P donor electron spins, spin-dependent excess charge-carrier recombination through so-called P_{b0} centres is used. P_{b0} centres are trivalent Si atoms at the interface between crystalline silicon (c-Si) and silicon dioxide (SiO_2) that introduce localized, paramagnetic states in the Si bandgap and dominate electron trapping and recombination at the interface[17,18]. If a neutral P_{b0} centre is located in the vicinity of a ^{31}P donor, the electron bound to the ^{31}P and the electron in the P_{b0} centre can form a coupled spin pair[19,20], whose wavefunction $|\Psi\rangle$ can exist in an arbitrary superposition of any of its four energy eigenstates. Two of these states, $|T_+\rangle = |\uparrow\uparrow\rangle$ and $|T_-\rangle = |\downarrow\downarrow\rangle$ (where the first arrow indicates the state of the ^{31}P electron spin and the second arrow the state of the P_{b0} spin) have triplet symmetry and are independent of the strength of the spin–spin coupling. The remaining two states depend on the coupling: For strong spin–spin interaction, they are the pure triplet $|T_0\rangle = (1/\sqrt{2})(|\uparrow\downarrow\rangle + |\downarrow\uparrow\rangle)$ and the singlet $|S\rangle = (1/\sqrt{2})(|\uparrow\downarrow\rangle - |\downarrow\uparrow\rangle)$ states, whereas in the absence of spin–spin coupling, they are product states $|\uparrow\downarrow\rangle$ and $|\downarrow\uparrow\rangle$ that can be represented by equal mixtures of $|T_0\rangle$ and $|S\rangle$. For the intermediate coupling regime, the energy eigenbase changes continuously between the two limiting cases. Once a spin pair is generated, it can relax by a transfer of the electron from the ^{31}P donor to the P_{b0}, forming a negatively charged P_{b0}^-. This relaxation transition depends strongly on the initial symmetry of the two spins within the pair. As the energetically lowest doubly occupied charged state of the P_{b0} has to be diamagnetic owing to the Pauli exclusion principle, the relaxation probability is proportional to the singlet content $|\langle S|\Psi\rangle|^2$ of the pair[20]. After subsequent capture of an excess hole by the P_{b0}^-, and an excess electron by the $^{31}P^+$, both centres

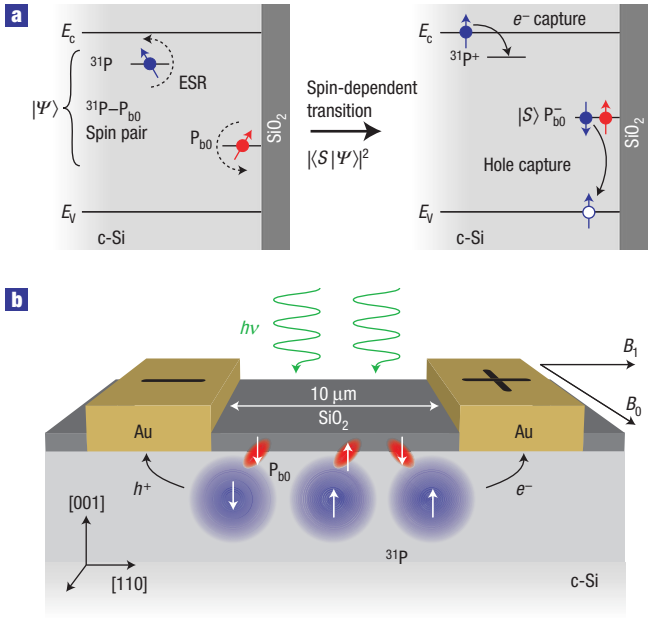

Figure 1 Readout scheme for ^{31}P electron spin quantum states via spin-dependent charge-carrier recombination at P_{b0} centres at the crystalline Si/SiO_2 interface. a, Band diagram of the Si/SiO_2 interface assuming flat band condition. The electrons at the ^{31}P donor and the P_{b0} centre form a weakly coupled spin pair $|\Psi\rangle$. As the negatively charged P_{b0}^- state is diamagnetic, the recombination probability is proportional to the singlet content $|\langle S|\Psi\rangle|^2$ of the initial pair. ESR of either constituent of the pair can therefore influence the recombination of excess charge carriers. **b**, Sample structure used for the experiments shown here. To preferentially locate ^{31}P in the vicinity of c-Si/SiO_2 states, the active sample is a 15-nm-thick epitaxial layer of ^{31}P-doped c-Si deposited on an intrinsic Si buffer layer. For the electrical measurement, gold contacts are deposited on top of the Si surface.

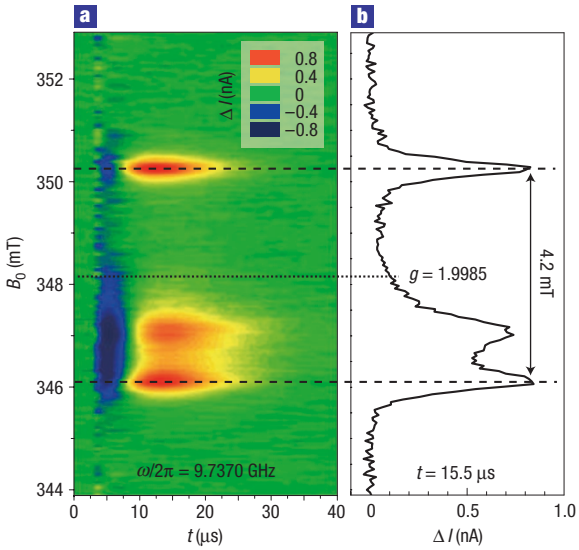

Figure 2 Pulsed electrically detected magnetic resonance of ^{31}P–P_{b0} pairs. **a**, Contour plot of the transient current change after a 480-ns-long microwave pulse with a power $P_{MW} = 1$ W as a function of the magnetic field B_0 and after subtraction of microwave artefacts. To protect the amplifier against overload, the detection system is activated only after 3 μs. **b**, Every time slice has the shape of an ESR spectrum, as exemplarily shown for $t = 15.5$ μs. The spectrum is a superposition of the hyperfine-split resonance of the ^{31}P donors and the resonance of the P_{b0} centres.

return to their initial uncharged states. This capture of mobile charge carriers, for example, generated by illumination, renders the spin-dependent process detectable by current measurements.

To demonstrate the feasibility of this readout scheme mapping the ^{31}P donor electron spin state on electrical current, pulsed electrically detected magnetic resonance experiments (pEDMR) were carried out on the test structure shown in Fig. 1b. A resonant microwave pulse is used to induce coherent manipulation of the electron spins by electron spin resonance (ESR). The resulting change of the recombination rate is then detected by a transient photoconductivity measurement after the coherent excitation is turned off[20]. For the preparation of the initial state of the ensemble of spin pairs, the sample is allowed to attain a low-temperature ($T = 5$ K) steady state in the presence of a strong offset photocurrent $I = 50$ μA, a constant magnetic field $B_0 \approx 350$ mT and illumination with a tungsten light source. In this way, a high density of $|T_+\rangle$ and $|T_-\rangle$ spin pairs is generated, as the steady-state recombination leads to a depletion of the short-lived pair states $|S\rangle$ and, in the case of intermediate or weak coupling, $|T_0\rangle$. pEDMR is induced by an intense, coherent ESR microwave pulse generated by a Bruker E580 pulse bridge and amplified by a 1 kW travelling-wave tube amplifier, which imposes a unitary transformation on the spin-pair eigenstates. The final state of this transformation is a coherent non-eigenstate, determined by adjustable pulse parameters such as intensity, pulse length and microwave frequency. If this state has an increased singlet content, the recombination rate after the pulse is also increased and will only gradually return to its steady state, as recombination processes of the charge-carrier pairs typically take place on a much slower timescale than their manipulation by the strong microwave pulse. Figure 2a shows a contour plot of the change ΔI of the photocurrent from its steady-state value as a function of time t after the microwave pulse was turned off. The data shown were obtained for different magnetic fields B_0 and represent the measured data after subtraction of non-resonant microwave artefacts. The contour plot shows three resonances at $B_0 = 346.2$ mT, $B_0 = 347.1$ mT and $B_0 = 350.3$ mT, also visible in Fig. 2b, which shows a time slice through the contour plot for $t = 15.5$ μs. The two features indicated by dashed lines have equal amplitudes, are separated by 4.2 mT and correspond to a central g value of 1.9985. This is the characteristic ESR hyperfine signature of the ^{31}P donor electron in silicon[21,22]. The broader peak at $B_0 = 347.1$ mT is an unresolved superposition of signal contributions from P_{b0} centres that have different orientations with respect to the Si(100) surface, which results in resonances at $g = 2.0039$ and $g = 2.0081$ for the orientation of the sample with respect to the magnetic-field orientation indicated in Fig. 1b (refs 17,18). The current transients at the three resonances exhibit identical dynamics: an initial strong photocurrent decrease caused by the higher singlet content followed by a slower increase of the current originating from the quenching of the number of triplet states that also have a finite recombination probability[20]. We conclude from the identical time dependence that the electronic transitions that cause the observed signals must belong to the same recombination process, involving ^{31}P donors and P_{b0} centres, as illustrated in Fig. 1.

The transient response of the photocurrent after the microwave pulse is proportional to the relative singlet density change induced by the microwave pulse[20]. Therefore, a current change, integrated over a certain time in a box-car type of experiment for the purpose

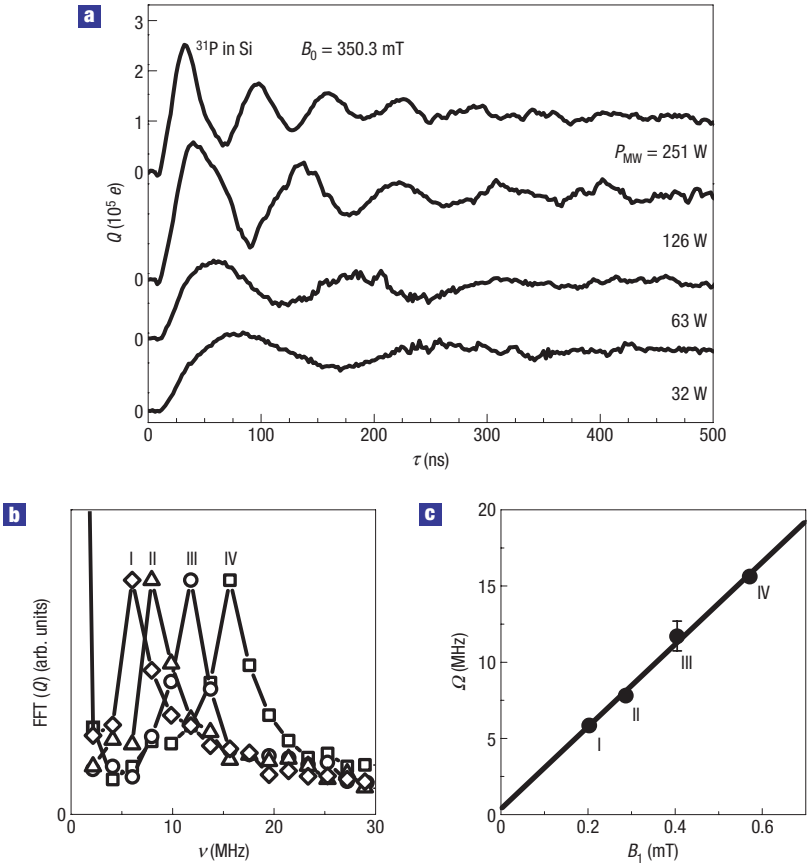

Figure 3 Electrical observation of Rabi flops of ^{31}P electron spins. **a**, Photoconductivity change integrated from $t_1 = 7\,\mu$s to $t_2 = 23\,\mu$s after a coherent ESR excitation as a function of the applied pulse length τ for four different microwave powers P_{MW}. **b**, FFT of $Q(\tau)$ for the four data sets shown in **a**, normalized to the intensity of the frequency peak. **c**, Peak frequencies Ω from **b** as a function of the microwave field amplitude B_1 showing the linear relationship expected for Rabi flops. The typical error bar in **c** indicates the resolution of the FFT caused by the maximum pulse length τ.

of noise reduction yielding a charge Q, reflects the spin-state densities directly after the pulse. Because a change of the pulse length τ causes a different nutation angle for the ^{31}P spin on resonance and thus a different singlet content for the ^{31}P–P_{b0} spin pair after the pulse, a measurement of $Q(\tau)$ must reveal the coherent Rabi nutation of the spins in resonance[23].

To observe Rabi flops of the ^{31}P electron spins, the transient current measurement was repeated on resonance with the ^{31}P peak at the magnetic field of $B_0 = 350.3$ mT under application of microwave pulses with different length τ. Figure 3a shows the measurement of $Q(\tau)$ obtained for four different pulse powers P_{MW} under otherwise identical experimental conditions as for the experiments shown in Fig. 2. We clearly see well-developed oscillations that increase in frequency for increasing microwave power. This can be seen more quantitatively in Fig. 3b, which shows the fast-Fourier transform (FFT) of $Q(\tau)$. These curves were normalized to the maximum of their respective frequency peaks. With increasing microwave field strength $B_1 \propto \sqrt{P_{MW}}$, we observe a clear shift of the characteristic oscillation frequency Ω to higher values. Figure 3c shows that the peak frequency increases linearly with the excitation field B_1, as expected for Rabi oscillations. For the integration times used in Fig. 3, a maximum of the recombining charge $Q(\tau)$ corresponds to a maximum of singlet states after the pulse. As at low temperatures the electron spins of ^{31}P and P_{b0} are in the $|\downarrow\downarrow\rangle$ triplet state before the pulse, the maximum of Q indicates $|\uparrow\rangle$ of ^{31}P after the pulse, a minimum corresponds to $|\downarrow\rangle$. Rabi echo experiments (not shown) reveal that the fast decay of the Rabi oscillations in Fig. 3a is not due to incoherence but is caused by an inhomogeneous B_1 field, which leads to a fast coherent dephasing of the spin ensemble.

On resonance, $\Omega = \gamma B_1$ should hold for isolated spin-1/2 states, where $\gamma = g\mu_B/\hbar$ is the gyromagnetic ratio, μ_B is the Bohr magneton and $\hbar$ is the reduced Planck constant. From the linear fit of the data shown in Fig. 3c, we obtain a proportionality factor of $\gamma_{exp} = (1.03 \pm 0.08)\gamma$. As the ratio $\Omega/\gamma B_1$ is greater than 1 for strongly coupled systems[24], the experimentally observed $\Omega/\gamma B_1 \approx 1$ indicates a weakly coupled spin pair.

Off resonance, the relation between the observed oscillation frequency Ω of $Q(\tau)$ and the applied B_1 field is described by the Rabi nutation frequency formula $\Omega = \sqrt{(\gamma B_1)^2 + (\omega - \omega_L)^2}$ in the limit of uncoupled spins[20,25]. Here, ω is the angular frequency of the microwave radiation and $\omega_L = \gamma B_0$ is the Larmor frequency of the spin. To test the Rabi frequency formula for spin-dependent recombination off resonance, Ω was measured with a fixed B_1 and varied B_0 (or Larmor frequency ω_L) near the high-field ^{31}P resonance. Figure 4 shows the results of these measurements in a contour plot of the FFT of $Q(\tau)$ as a function of B_0. A symmetric increase of Ω with increasing distance from the resonance peak is observed in full agreement with the predictions for Ω at $g = 1.9985$, indicated by the white line. Therefore, the oscillations of $Q(\tau)$ shown in Figs 3 and 4 fully meet the predictions of Rabi oscillations of weakly coupled spin-1/2 states.

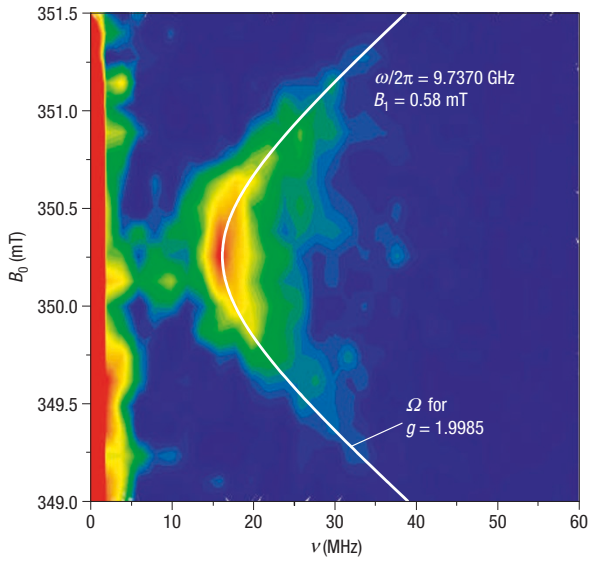

Figure 4 Detuning-induced shift of the Rabi nutation frequency. The contour plot shows the FFT of $Q(\tau)$ as a function of the applied magnetic field B_0 in the vicinity of the high-field ^{31}P resonance. The data confirm the predictions for the off-resonance Rabi frequency Ω of a weakly coupled spin-1/2 system with $g = 1.9985$ indicated by the white solid line. The colour scale is in arbitrary units.

The experiments shown here have been carried out on ensembles of ^{31}P donors. The charge noise achieved so far is about 10^4 e, as shown in Fig. 3. As the flip of a single spin approximately leads to one elementary charge detected in the box-car pEDMR experiment[20], the detection limit of pEDMR demonstrated here is around 11 orders of magnitude lower than for conventional nuclear magnetic resonance and about 7 orders of magnitude lower than for ESR[26]. The noise is most likely determined by the shot noise of shunt currents due to excess charge carriers that diffuse into the c-Si bulk. Suppression of these currents via improved sample geometry, for example, using a buried oxide and lateral structuring for confinement should reduce the noise level, resulting in an even higher sensitivity. In fact, continuous-wave EDMR was recently used to successfully detect as few as 100 ^{31}P atoms implanted into intrinsic c-Si (ref. 27).

The experimental results shown are an important step towards the realization of an electrical spin readout of donors. The proof-of-principle experiments demonstrate a spin-to-charge transfer mechanism required for ^{31}P electron spin readout via ^{31}P–P_{b0} pairs and show that this spin pair is sufficiently weakly coupled so that the ^{31}P hyperfine interaction can be observed, ultimately allowing the electrical detection of the nuclear spin state[28]. However, although inclusion of this readout scheme into a scalable architecture is in principle conceivable via local gates electrostatically controlling the ^{31}P–P_{b0} coupling, there remain a variety of physical and technological issues such as the positioning of P_{b0} centres as well as decoherence by the c-Si/SiO_2 interface[29] or by light-induced charge carriers that have to be addressed before application of the readout scheme to quantum information processing.

METHODS

The test structures investigated were grown by low-pressure chemical vapour deposition. The sample consists of a 15-nm-thick layer of c-Si doped with 10^{17} cm^{-3} ^{31}P atoms on a 5 μm intrinsic buffer. The substrate is a 30-Ω-cm boron-doped Si(001) wafer. A high density of P_{b0} centres is achieved by using a native oxide for the formation of the Si/SiO_2 interface. The electrical contacts are a grid structure consisting of 10-nm-thick chromium and 100-nm-thick gold films and comprising 112 digits of 2 mm length, 10 μm width and 10 μm spacing.

Received 7 August 2006; accepted 25 October 2006; published 19 November 2006.

References

1. Elzerman, J. M. *et al.* Single-shot read-out of an individual electron spin in a quantum dot. *Nature* **430,** 431–435 (2004).
2. Petta, J. R. *et al.* Coherent manipulation of coupled electron spins in semiconductor quantum dots. *Science* **309,** 2180–2184 (2005).
3. Mooij, J. E. *et al.* Josephson persistent-current qubit. *Science* **285,** 1036–1039 (1999).
4. Pashkin, Y. A. *et al.* Quantum oscillations in two coupled charge qubits. *Nature* **421,** 823–826 (2003).
5. Kennedy, T. *et al.* Single-qubit operations with the nitrogen-vacancy center in diamond. *Phys. Status Solidi B* **233,** 416–426 (2002).
6. Jelezko, F. *et al.* Observation of coherent oscillation of a single nuclear spin and realization of a two-qubit conditional quantum gate. *Phys. Rev. Lett.* **93,** 130501 (2004).
7. Kane, B. E. A silicon-based nuclear spin quantum computer. *Nature* **393,** 133–137 (1998).
8. Kane, B. E. Silicon-based quantum computation. *Fort. Phys.* **48,** 1023–1041 (2000).
9. Vrijen, R. *et al.* Electron-spin-resonance transistors for quantum computing in silicon-germanium heterostructures. *Phys. Rev. A* **62,** 012306 (2000).
10. Hollenberg, L. C. L. *et al.* Charge-based quantum computing using single donors in semiconductors. *Phys. Rev. B* **69,** 113301 (2004).
11. Clark, R. G. *et al.* Progress in silicon-based quantum computing. *Phil. Trans. R. Soc. Lond. A* **361,** 1451–1471 (2003).
12. Xiao, M., Martin, I., Yablonovitch, E. & Jiang, H. W. Electrical detection of the spin resonance of a single electron in a silicon field-effect transistor. *Nature* **430,** 435–439 (2004).
13. Brandt, M. S. *et al.* Spin-dependent transport in elemental and compound semiconductors and nanostructures. *Phys. Status Solidi C* **1,** 2056–2078 (2004).
14. Boehme, C. & Lips, K. Spin-dependent recombination—an electronic readout mechanism for solid state quantum computers. *Phys. Status Solidi B* **233,** 427–435 (2002).
15. Schmidt, J. & Solomon, I. Modulation de la photoconductivité dans le silicium à basse température par résonance magnétique électronique des impuretés peu profondes. *C.R. Acad. Sci. B* **263,** 169–172 (1966).
16. Boehme, C. & Lips, K. Electrical detection of spin coherence in silicon. *Phys. Rev. Lett.* **91,** 246603 (2003).
17. Poindexter, E. H., Caplan, P. J., Deal, B. E. & Razouk, R. R. Interface states and electron spin resonance centers in thermally oxidized (111) and (100) silicon wafers. *J. Appl. Phys.* **52,** 879–884 (1981).
18. Stesmans, A. & Afanes'ev, V. V. Electron spin resonance features of interface defects in thermal (100) Si/SiO_2. *J. Appl. Phys.* **83,** 2449–2457 (1998).
19. Kaplan, D., Solomon, I. & Mott, N. F. Explanation of the large spin-dependent recombination effect in semiconductors. *J. Phys. Lett. (Paris)* **39,** L51–L54 (1978).
20. Boehme, C. & Lips, K. Theory of time-domain measurement of spin-dependent recombination with pulsed electrically detected magnetic resonance. *Phys. Rev. B* **68,** 245105 (2003).
21. Feher, G. Electron spin resonance experiments on donors in silicon. I. Electronic structure of donors by the electron nuclear double resonance technique. *Phys. Rev.* **114,** 1219–1244 (1959).
22. Young, C. F. & Poindexter, E. H. Electron paramagnetic resonance of conduction-band electrons in silicon. *Phys. Rev. B* **55,** 16245–16248 (1997).
23. Boehme, C. & Lips, K. The ultrasensitive electrical detection of spin–Rabi oscillation at paramagnetic defects. *Physica B* **376,** 930–935 (2006).
24. Rajevac, V. *et al.* Transport and recombination through weakly coupled localized spin pairs in semiconductors during coherent spin excitation. *Phys. Rev. B* (in the press); preprint at <http://arxiv.org/abs/cond-mat/0607627> (2006).
25. Rabi, I. I. Space quantization in a gyrating magnetic field. *Phys. Rev.* **51,** 652–654 (1937).
26. Maier, D. C. New frontiers in x-band cw-epr sensitivity. *Bruker Rep.* **144,** 13–15 (1997).
27. McCamey, D. R. *et al.* Electrically detected magnetic resonance in ion-implanted Si:P nanostructures. *Appl. Phys. Lett.* **89,** 182115 (2006).
28. Machida, T., Yamazaki, T., Ikushima, K. & Komiyama, S. Coherent control of nuclear-spin system in a quantum-Hall device. *Appl. Phys. Lett.* **82,** 409–414 (2003).
29. Schenkel, T. *et al.* Electrical activation and electron spin coherence of ultralow dose antimony implants in silicon. *Appl. Phys. Lett.* **88,** 112101 (2006).

Acknowledgements

This work was financially supported by Deutsche Forschungsgemeinschaft through SFB 631. The sample investigated was grown by G. Vogg and F. Bensch at Fraunhofer IZM in Munich. Correspondence and requests for materials should be addressed to A.R.S. or C.B.

Competing financial interests

The authors declare that they have no competing financial interests.